Supporting Information

Tasaki et al. 10.1073/pnas.1217358110

SI Results

Yolk Sac Vascular Defects Are the Primary Cause of Death in UBR4-Deficient Mouse Embryos. It is challenging to dissect phenotypes of genetically engineered mouse embryos that die during embryogenesis as multiple misregulations may interfere with each other. We suggest that UBR4-deficient mouse embryos die primarily due to vascular defects in the yolk sac (YS) based on the following reasons. First, embryonic death at approximately embryonic day 9.5 (E9.5)–E10.5 is typically caused by cardiovascular defects because most of noncardiovascular organs at this stage, such as liver, brain, kidney, and pancreas, are not functional yet and, thus, are not required for survival at E9.5–E10.5. Second, defects in cardiac development do not cause lethality at E9.5–E10.5 because the heart is also not functional at this stage. Third, because the placenta that provides maternal nutrients and gases to the embryo is not functional at E9.5–E10.5, the embryo must be supplied with nutrients, amino acids, and gases exclusively from the YS. As such, the death of mouse embryos at this stage is typically caused by circulation defects, either in the YS or embryo. Fourth, our results suggest that vascular defects are more severe in the yolk sac compared with the embryonic body. Fifth, the severity of yolk sac vascular defects tightly correlates to the timing of embryonic death and the severity of developmental arrest. Sixth, UBR4 is more prominently expressed in the yolk sac relative to the embryonic body. Seventh, UBR4-deficient yolk sac shows normal rates of cell proliferation (Fig. 2*L*) and death (Fig. 2*M*).

Misregulation of Autophagy in the YS Endoderm Contributes to the Vascular Failure in the YS Mesoderm. As illustrated in Fig. S2, the YS endoderm has a specialized proteolytic system that internalizes, delivers (via multivesicular bodies, MVBs), and digests maternal proteins using hydrolases of professionally enlarged lysosomes. The resulting lysosome-derived amino acids are: (*i*) used to synthesize grow factors to orchestrate vascular development in the YS mesoderm, (*ii*) supplied to the underlying YS mesodermal layer to synthesize protein in vascular development, and (*iii*) supplied to the embryos for protein synthesis during embryogenesis. Our results show that: (*i*) the level of UBR4 in the YS mesoderm is nondetectible, (*ii*) UBR4 marks the YS endoderm, (*iii*) UBR4 forms cytosolic punctate structures that colocalize with LC3 puncta, (*iv*) UBR4 puncta have size and shape distinct from those of LC3 puncta, (*v*) UBR4-deficient YSs show an increased level of puncta of LC3 and ATG12, and (*vi*) UBR4 is found within the MVB in cultured cells. Taken together, it is likely that misregulation in autophagic degradation of cargoes (including maternal proteins) causes stress in the YS endoderm, which in turn affects vascular development in the YS mesoderm.

UBR4 Subpopulation Is Degraded by Autophagy Through Its Association with Autophagic Cargoes. As UBR4 is a huge protein with a size of 570 kDa, a portion of UBR4 stably expressed in HEK293 cells may be deposited to autophagic vacuoles as misfolded aggregates. Nonetheless, several lines of evidence suggest that the majority of UBR4 molecules are first associated with (unidentified) cellular cargoes to form UBR4–cargo complexes destined to autophagic vacuoles. First, the majority of UBR4 in HEK293–UBR4V5 cells is retrieved from cytosolic and ER membrane fraction and can be solubilized with a nonionic detergent (Fig. S6). Second, the EM staining study of UBR4 invariably revealed one or a few individually isolated dots (not as aggregates) associated with cellular cargoes or autophagic vacuoles (Fig. 3 *G* and *H*). Third, transient expression of UBR4V5 resulted in the formation of $UBR4V5^{+}LC3^{-}$ puncta both in mouse embryonic fibroblasts (MEFs) (Fig. S8) and HEK293 cells (Fig. S9), which are likely to represent $UBR4V5^{+}$ cellular cargoes that have not been delivered to autophagic vacuoles. Fourth, cytosolic puncta positive for "endogenous" UBR4 in the visceral YS show shapes and sizes distinct from those of ATG12, ATG5, and LC3 (Fig. 3 *D–F*, arrowheads). In addition, a confocal distance measurement indicated that the center of UBR4 puncta is separated from that of LC3 puncta by ~0.15 μm. Fifth, endogenous UBR4 is a relatively stable protein in MEFs (Fig. 3*N*), and its autophagic degradation is accelerated by nutrient deprivation (Fig. 3*N*). A protein prone to misfolding is expected to be constitutively degraded.

SI Materials and Methods

Construction of Mice Lacking UBR4. We cloned the *UBR4* gene from a bacterial artificial chromosome (BAC) library (CITB; Invitrogen) derived from the mouse embryonic stem (ES) cell line CJ7 using a mouse *UBR4* cDNA fragment (nucleotides 4231–5430) as a probe. The interval ribosome entry site (IRES)-taulacZ-pA-ACNF plasmid, derived from the IRES-taulacZ-pA cassette (1) and the ACNF cassette (2), is a gift from Peter Mombaerts (Rockefeller University, New York). The targeting vector pUBR4KO-tauLacZ was constructed using gene recombineering (recombination-mediated genetic engineering) as described (3, 4), linearized with FseI, and electroporated into E14 ES cells (a gift from Peter Mombaerts). Targeted ES cell clones were analyzed using Southern blotting and PCR analysis. The clone 2F12 ES cells were injected into C57/BL6J blastocysts to generate chimeric mice, which, in turn, were used to obtain germ-line transmission of the $UBR4^{-}$ mutant allele.

Antibodies. Rabbit polyclonal anti-human UBR4 antibody (1:400), raised against residues 3755–4160 (5), was used for immunostaining of the YS. Rabbit polyclonal anti-UBR4 antibody (1:300, IHC-00640; Bethyl Laboratories) was used for immunostaining of cultured cells. Other primary antibodies are rabbit polyclonal anti-V5 (1:500, V8137; Sigma), goat polyclonal anti-ATG12 (1:100, SC-70128; Santa Cruz Biotechnology), goat polyclonal anti-ATG5 (1:200, SC-8666; Santa Cruz Biotechnology), rat anti-BrdU (1: 100, H9367; Accurate Chemical & Scientific), mouse monoclonal anti–α-SMA (1:400, A2547; Sigma), rat monoclonal anti–PECAM-1 (1:300, MEC13.3; Pharmingen), and goat polyclonal anti-LC3 (1:100, SC-16755; Santa Cruz Biotechnology). Antibodies for immunoblotting analysis are anti-LC3 (1:2,000, L7543; Sigma), p62 (1:5,000, GP92-C; Progen), GABARAP (OSG00009W; Thermo Scientific, 1:1,000), V5 (1:2,000; Invitrogen), and β-actin (1:100,000, A1978; Sigma). The following secondary antibodies are from Invitrogen: Alexa Fluor 488 goat anti-rabbit IgG (1:200, A11034), Alexa Fluor 555 donkey anti-goat IgG (1:200, A21432), Alexa Fluor 555 goat anti-mouse IgG (1:200, A21424), and anti-rat IgG-HRP (1: 500; Jackson ImmunoResearch).

Reverse Transcriptase-PCR Analysis. Total RNA was prepared from a pool of five E9.5 embryos for each of +/+ and $UBR4^{-/-}$ genotypes using TRIzol (Invitrogen) and RNeasy kit (Qiagen). The first cDNA strand was synthesized using SuperScript III reverse transcriptionase (Invitrogen) and hexamer random oligos. Reverse transcription for quantitative PCR was performed using the iScript cDNA synthesis kit (Bio-Rad). Quantitative PCR was performed in duplicates by using Platinum SYBR Green (Invitrogen)

with ABI 7300/7500 real-time PCR system and primer sequences listed in Table S2.

Histology and β-Galactosidase Staining. For histological analysis, embryos were fixed overnight at 4 °C in 4% paraformaldehyde in PBS. Embryos were treated with 70% ethanol, dehydrated, embedded in paraffin wax, and sectioned transversely or sagittally with 7 μm thickness, followed by staining with hematoxylin and eosin (H&E). To detect the activity of β-galactosidase on sections, embryos or tissues were fixed in 0.25% glutaraldehyde for 5 min, rinsed in PBS three times, and stained overnight at 37 °C in X-gal solution (1.3 mg/mL potassium ferrocyanide, 1 mg/mL potassium ferricyanide, 0.3% Triton X-100, 1 mM $MgCl_2$, 150 mM NaCl, and 1 mg/mL 4-choloro-5-bromo-3-indolyl-β-galactoside (X-gal; Roche Applied Science) in PBS (pH 7.4), followed by postfixation.

Immunohistochemistry. For immunohistochemistry of animal tissues, paraffin-embedded slides were treated with xylene, followed by gradual dehydration in EtOH (100%, 90%, 80%, and 70%; 6 min each) and rehydration in water for 20 min. The slides were treated with blocking solution (1% BSA and 0.2% Triton X-100 in PBS) for 1 h and incubated with primary antibodies and subsequently secondary antibodies. Confocal images were taken with a Fluoview FV1000 confocal laser scanning microscope equipped with Olympus Plan-Apo 60× (1.42 NA) oil immersion lens and analyzed using Fluoview software (Olympus). Two ImageJ (1) plugins, colocalization finder (by Christophe Laummonerie and Jerome Mutterer) and JACoP (Just Another Colocalization Plugin, 2), were used to evaluate colocalization of fluorescent images.

Immunoelectron Microscopy. HEK293–UBR4V5 cells were fixed in 2% PFA in PBS, pH 7.4, for 1 h and washed with PBS. Fixed cells were collected by scraping and resuspended in 3% gelatin. The gelatin was solidified on ice, and cells embedded in gelatin were fixed again with 2% PFA for 15 min. After cryoprotected with 2.3 M sucrose with PVP solution overnight, samples were frozen in liquid nitrogen and trimmed into 0.5-mm cubes. The frozen cell blocks were sectioned by cryomicrotome (Leica EM Crion) in 70-nm sections and collected on 200-mesh grids. Primary antibodies were diluted in 0.1 M PBS with 0.5% BSA and 0.15% glycine. Donkey anti-rabbit 12 nm gold beads and donkey anti-goat 18 nm gold beads were diluted to 1:25 before use. After immunostaining, sections were incubated with 2.5% glutalaldehyde for 10 min and with 2% neutral UA acetate for 7 min. Sections were further processed with 4% uranyl acetate and methyl cellulose for contrasting and drying, respectively. After drying, samples were recorded using JEOL JEM1011 TEM with a high-resolution AMT digital camera.

Establishment of *UBR4*$^{-/-}$ MEFs. Primary MEFs were established from E8.5 *UBR4*$^{-/-}$ embryos and their +/+ littermates. The embryos were minced by pipetting in Iscove's modified Dulbecco's medium (IMDM) (31980–022; Invitrogen), 15% FBS (HyClone), 0.1 mM nonessential amino acids (Invitrogen), 0.1 mM β-mercaptoethanol, and 100 units/mL penicillin/streptomycin (Invitrogen). The cells were seeded on the gelatinized 35-mm culture dish. Permanent cell lines were established from primary MEFs through crisis-mediated immortalization over 10 passages.

Proximity Ligation Assay. The proximity ligation assay (PLA) was used to visualize protein–protein interactions in UBR4V5 stable HEK293 cells using a reagent kit (Olink Bioscience). The cells were fixed with 4% paraformaldehyde for 0.5 h and blocked for 1 h in 10% goat serum (Invitrogen), followed by incubation with UBR4 and test antibodies (ATG12 or LC3) in antibody solution (0.3% Triton X-100 and 5% BSA in PBS) overnight at 4 °C. The cells were incubated with two oligonucleotide-tagged probe antibodies against primary antibodies. Annealing of the probes occurs when the target proteins are within 400 Å from each other, which initiates the amplification of green fluorophore. Following a 1-h incubation with the PLA probes, the cells were subject to hybridization, ligation, and DNA amplification in accordance with the manufacturer's instruction. A z-stack image of the green PLA signals was obtained by combining 20 focal planes (0.53 μm/slice) using a confocal microscope (Olympus; FV1000).

In Vivo Proliferation Assay. In vivo proliferation assay was performed as described. Pregnant mice were intraperitoneally injected (150 mg/g) with 5-bromo-2-deoxyuridine (BrdU) in 250 μL saline. After 2 h postinjection, embryos were subjected to paraffin sectioning and immunostaining BrdU (S phase marker).

Knockdown of UBR4. HEK293 cells were transfected with control (4390843) or UBR4 siRNA (4392420, ID 23628) from Life Technologies at a final concentration of 10 nM using Lipofectamine RNAiMAX reagent (13778150). After 48 h post-siRNA transfection, the cells were transfected with pcDNA6.2-cluv-hUBR4V5 and/or vector plasmid using Lipofectamine LTX (15338100). After 24 h postplasmid transfection (total 72 h after siRNA treatment), the cells were subjected to immunocytochemistry (see below) or immunoblotting using RIPA buffer (150 mM NaCl, 50 mM Tris·HCl, pH 8.0, 1% Nonidet P-40, 0.5% sodium deoxycholate, and 0.1% SDS) supplied with a protease inhibitor mixture (1:100; Sigma; P8340).

Immunocytochemistry of Cultured Cells. Coverslips (22 mm^2) placed in a six-well plate were incubated with diluted poly-L-lysine (1:10 in sterile deionized water) for 30 min at room temperature. After washing, the plate was exposed under a UV radiation lamp overnight in a hood. Cells were cultured and fixed in 4% paraformaldehyde in PBS (pH 7.4) for 0.5 h at room temperature. After washing twice with PBS, the cells were treated with blocking solution (5% FBS and 0.3% Triton X-100 in 0.1 M PBS) for 1 h, followed by incubation with primary and, subsequently, secondary antibodies. To induce starvation, the cells were washed twice with PBS and incubated in HBSS.

1. Mombaerts P, et al. (1996) Visualizing an olfactory sensory map. *Cell* 87(4):675–686.
2. Bunting M, Bernstein KE, Greer JM, Capecchi MR, Thomas KR (1999) Targeting genes for self-excision in the germ line. *Genes Dev* 13(12):1524–1528.
3. Liu P, Jenkins NA, Copeland NG (2003) A highly efficient recombineering-based method for generating conditional knockout mutations. *Genome Res* 13(3):476–484.
4. Warming S, Costantino N, Court DL, Jenkins NA, Copeland NG (2005) Simple and highly efficient BAC recombineering using galK selection. *Nucleic Acids Res* 33(4):e36.
5. Shim SY, et al. (2008) Protein 600 is a microtubule/endoplasmic reticulum-associated protein in CNS neurons. *J Neurosci* 28(14):3604–3614.

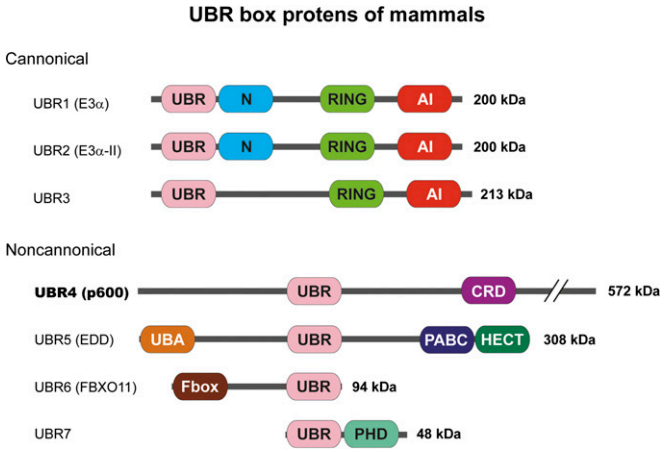

Fig. S1. The UBR box N-recognin family of the mammalian N-end rule pathway. AI, autoinhibitory domain; CRD, cystein-rich domain; Fbox, F-box; HECT, homologous to the E6-AP carboxyl terminus; N, N-domain; PABC, poly(A) binding protein C-terminal domain; PHD, plant homeodomain finger; RING, RING finger; UBA, ubiquitin association domain; UBR, UBR box.

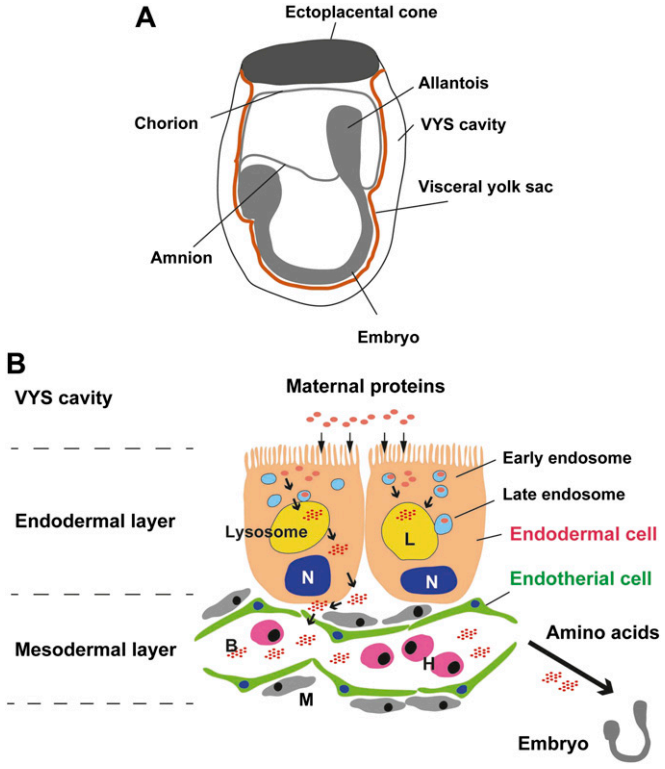

Fig. S2. Structure and function of the visceral yolk sac of murine embryos. (*A*) Developing structure of mouse embryo at E8.5. The visceral yolk sac functions as an early placenta, which exchanges nutrient and waste between E5.0 and E10 in mice. The yolk sac is also the first site where precursors of the erythroid cell lineage develop. (*B*) Illustration of layers of the visceral yolk sac (VYS) in mice. Maternal proteins are absorbed via microvilli on the apical surface of the endodermal cell layer of the VYS. Endocytosed maternal proteins are transferred to the lysosome through the early and late endosomes. In the lysosome, the maternal proteins are digested and secreted into the blood vessels in the mesenchymal cell layer. Digested amino acids are delivered to the embryo via the vitelline circulation. B, blood vessel; H, hematopoietic cell; L, lysosome; M, mesenchymal cell; N, nucleus.

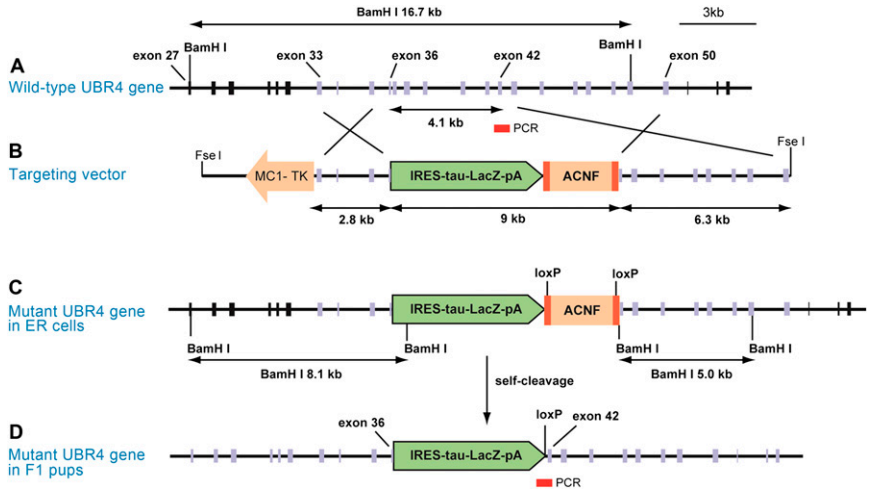

Fig. S3. Targeting strategy of the *UBR4* gene using recombineering. (*A*) Restriction map of the ~7.5-kb 5′-proximal region of the ~108-kb mouse *UBR4* gene spanning exons 27 through 53. (*B*) Targeting vector. (*C*) Targeted *UBR4*$^{-}$ allele in ES cells. (*D*) Targeted *UBR4*$^{-}$ allele in F_1 pups. Exons are denoted by solid vertical rectangles. Directions of transcription of the neomycin (*neo*) and the thymidine kinase (*tk*) genes are indicated. Homologous recombination resulted in the replacement of the *UBR4* exons 36–42 with the *neo* cassette. Exons 36 and 37, marked by an asterisk, contain Gly and Asp that are conserved in the UBR box N-recognin family and are essential for binding to type-1 destabilizing N-terminal residues in *Saccharomyces cerevisiae* Ubr1. Primers used for PCR genotyping are indicated by solid rectangles.

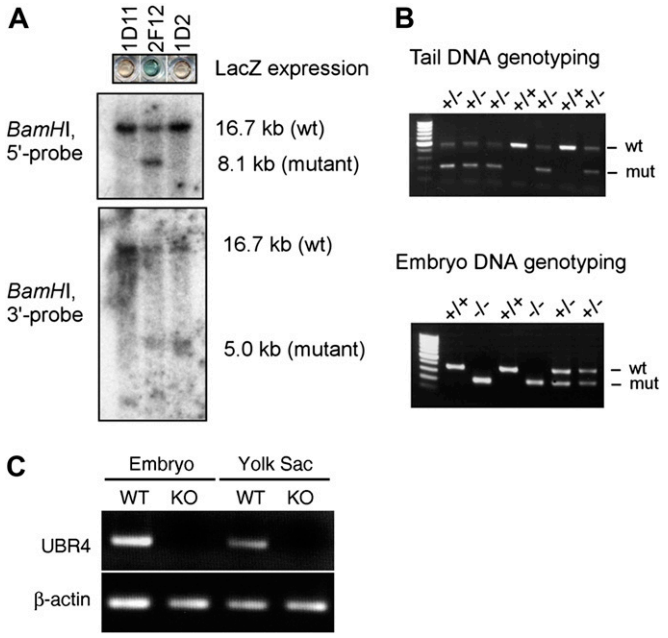

Fig. S4. Construction of UBR4-deficient mice. (*A*) Southern analysis of BamHI-cut DNA from the ES cell clones 1D11, 2F12, and 1D2. The 5′-probe detects 16.7 kb (wild-type) and 8.1 kb (*UBR4*$^{-}$ allele) diagnostic fragments. The 3′-probe detects 16.7 kb (wild-type) and 5.0 kb (*UBR4*$^{-}$ allele) diagnostic fragments. (*B*) PCR analysis of mouse tail DNA. (*C*) Semiquantitative PCR analysis of *UBR4* mRNA in +/+ (WT) and *UBR4*$^{-/-}$ (KO) embryos. Total RNA was isolated from embryonic bodies and YS.

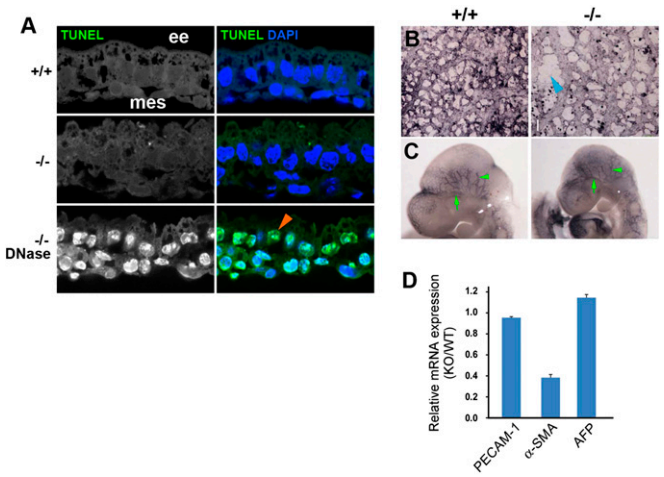

Fig. S5. Defective YS vascular development of UBR4-deficient embryos. (*A*) TUNEL assay of +/+ and *UBR4*$^{-/-}$ YS at E9.5. ee, extraembryonic endoderm; mes, mesodermal layer. Arrowhead, TUNEL^{+} cells in a positive control experiment. (*B*) Whole mount PECAM-1 staining of control and *UBR4*$^{-/-}$ YS at E9.5. Arrowheads indicate some of the differences in the branching patterns, relative to wild-type embryos. (Scale bars, 100 μm.) (*C*) Whole mount PECAM-1 staining of heads of +/+ and *UBR4*$^{-/-}$ embryos at E9.5. Arrowhead, the intracranial artery. (*D*) Real-time PCR analysis of PECAM-1, α-SMA, and AFP in +/+ and *UBR4*$^{-/-}$ YS at E9.5.

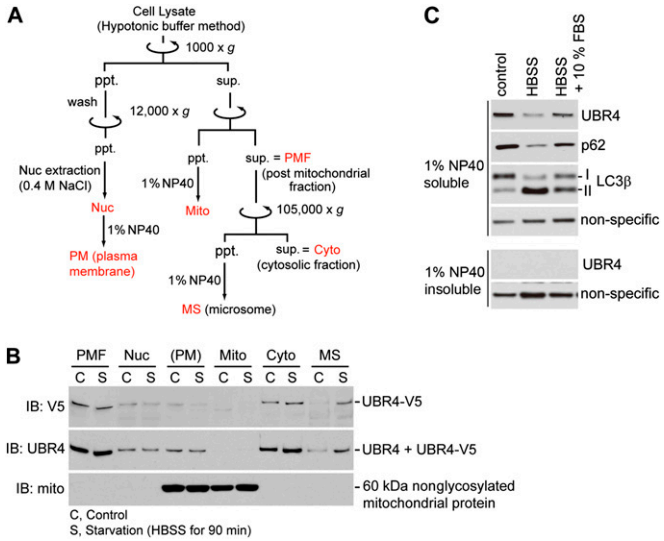

Fig. S6. UBR4 is a soluble protein. (*A*) Fractionation strategy. HEK293–UBR4V5 cells were harvested after starvation or control treatment and proteins and cellular proteins were fractionated by a differential centrifugation as described. (*B*) Western blot analysis. After fractionation, solubilized proteins were separated by SDS/PAGE and specific proteins were detected by anti-V5, anti-UBR4, and antimitochondrial proteins. (*C*) Extraordinarily large-sized UBR4 protein can be degraded through autophagy upon starvation without forming aggregates. Immunoblotting of soluble and insoluble proteins from MEFs in normal media or HBSS for 90 min. Cells were lysed using 1% Nonidet P-40 and insoluble proteins were separated by centrifugation. Results of 1% Nonidet P-40 soluble are also shown in Fig. 3*M*. Nonspecific (ns) signals were taken from anti-UBR4 blots. Cells were lysed by adding cold 1% Nonidet P-40 containing buffer with protease inhibitors and total lysate was collected by scraping. Insoluble fraction was separated by 12,000 × *g* centrifugation and resuspended with SDS-sample buffer before denaturation.

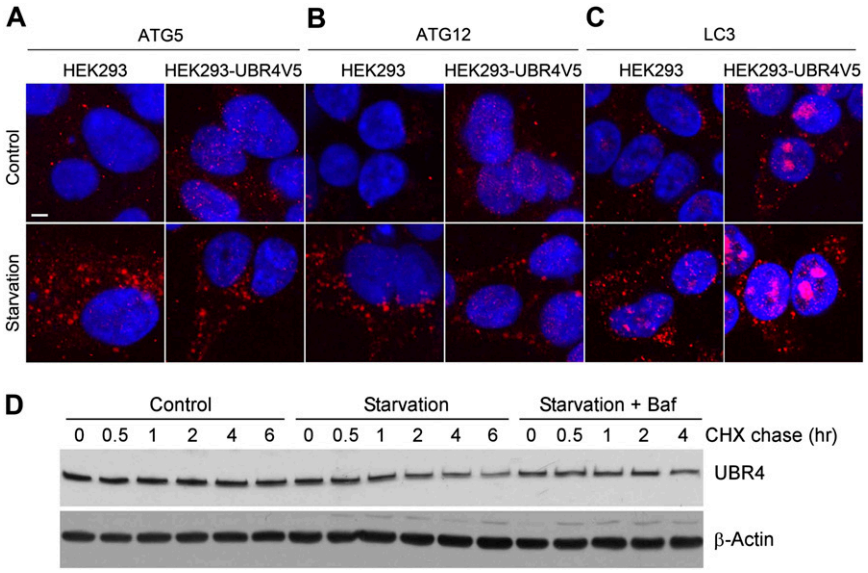

Fig. S7. The function of UBR4 in autophagy of cultured cells and its turnover by autophagy. (*A*–*C*) Stably expressed UBR4V5 induces the formation of puncta positive for ATG5, ATG12, and LC3. HEK293 and HEK293–UBR4V5 cells were immunostained for ATG5 (*A*), ATG12 (*B*), and LC3 (*C*). (Scale bars, 5 μm.) (*D*) Cyclohexamide-chase assay of UBR4 in MEFs. Cells were cultured in normal or starvation medium for 6 h in the presence of cycloheximide. Shown is a representative blot image from three independent experiments.

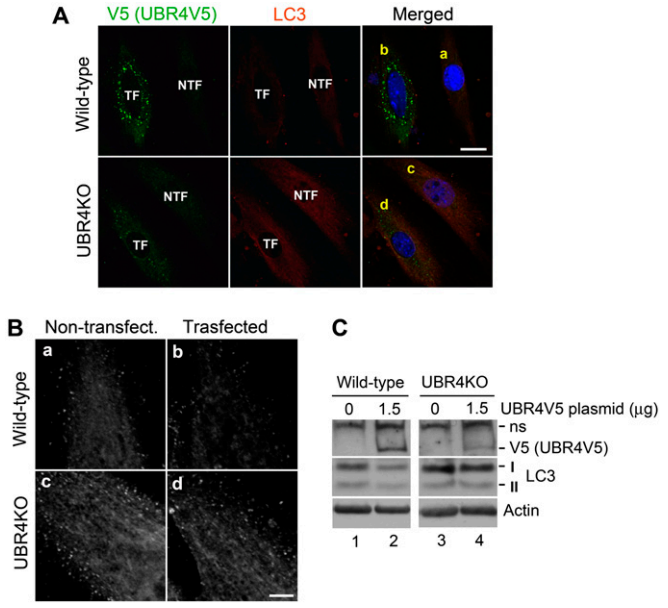

Fig. S8. Expression and conversion of LC3 in +/+ and UBR4-deficient MEFs transiently expressing UBR4V5. (*A*) Immunofluorescent analysis of V5 (UBR4V5) and LC3 in +/+ and UBR4-deficient MEFs transiently transfected with a plasmid encoding UBR4V5. Wild-type and UBR4-deficient MEFs were transfected with a plasmid (1.0 μg) encoding UBR4V5. One day after transfection, both transfected (TF) and nontransfected (NTF) cells were trypsinized, mixed, and replated on six-well dishes. This procedure minimizes individual variations between transfected and nontransfected cells. Note that LC3-I is accumulated in *UBR4*$^{-/-}$ MEFs growing in normal media, compared with +/+ MEFs, and that transient expression of UBR4V5 in *UBR4*$^{-/-}$ MEFs only marginally reduces the synthesis of LC3-I and the formation of LC3 foci. This marginal effect is consistent with a possibility that autophagic induction in *UBR4*$^{-/-}$ cells is caused by cellular stress and/or impairment of organelles that cannot be readily rescued by transient supplement of UBR4 for less than 24 h. Also note that transient expression of UBR4V5 in wild-type MEFs results in the formation of UBR4V5^{+}LC3^{-} puncta, which are likely to represent UBR4V5^{+} cellular cargoes that have not been delivered to autophagic vacuoles. (Scale bar, 20 μm.) (*B*) Enlarged views of the cellular areas indicated by *a*–*d*. (*a*) Nontransfected wild-type cell. (*b*) Transfected wild-type cell. (*c*) Nontransfected UBR4-deficient cell. (*d*) Transfected UBR4-deficient cell. (Scale bar, 4 μm.) (*C*) Immunoblotting analysis of V5 (UBR4V5) and LC3 in +/+ and UBR4-deficient MEFs transiently transfected with the indicated amounts of a plasmid encoding UBR4V5.

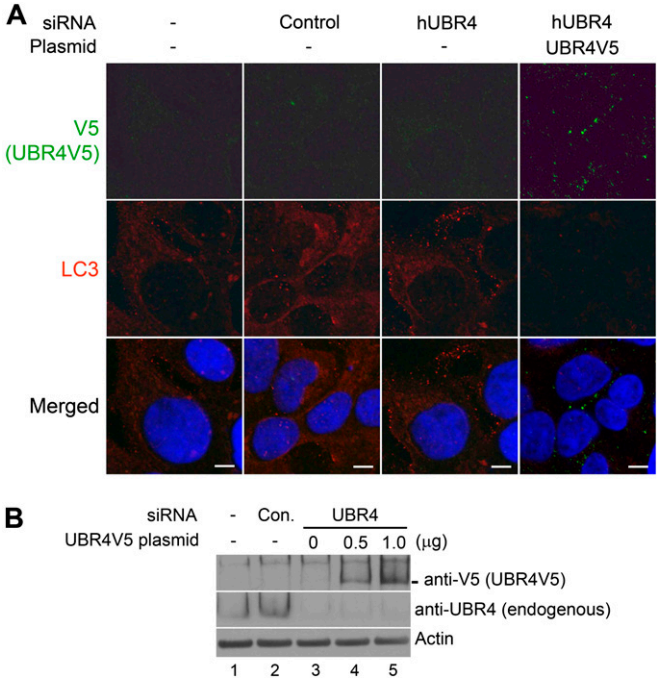

Fig. S9. Knockdown of UBR4 induces the formation of LC3 puncta in HEK293 cells. (*A*) HEK293 cells were transfected with control or UBR4 siRNA. After 48 h post-siRNA transfection, the cells were transfected with 1 μg pcDNA6.2-cluvhUBR4V5. After 24 h postplasmid transfection, the cells were subjected to immunocytochemistry of V5 and LC3. (Scale bar, 5 μm.) (*B*) Immunoblotting analysis of HEK293 cells that had been treated with UBR4 siRNA for 48 h, followed by transient transfection of the plasmid pcDNA6.2-cluvhUBR4V5. Note that overexpression of UBR4V5 in UBR4 knockdown cells results in disappearance of endogenous human UBR4 and accumulation of recombinant human UBR4V5.

Table S1. Genotyping of embryos from *UBR4*$^{+/-}$ intercrosses

Stage	+/+	+/–	–/–	ND	No. of litters	Averge litter size
E8.5	27	39	22		10	8.8
E9.0	13	23	12*		5	9.6
E9.5	43	107	40*	3	23	8.4
E10.5	7	17	6*	3	4	8.3
E11.5	6	8, 2†	3†		2	6.0
E12.5	3	5	0		1	8.0
E15.5	1	2	0		1	3.0
P21	65	138	0		35	5.8

ND, not determined.
*Morphologically abnormal.
†Found dead.

Table S2. Primers used for PCR analysis

Gene	Primer	Sequence
PECAM-1	PECAM-1–F	GAGCCCAATCACGTTTCAGTTT
	PECAM-1–R	TCCTTCCTGCTTCTTGCTAGCT
β-Actin	β-ACTIN–F	TGTGATGGTGGGAATGGGTCAGAA
	β-ACTIN–R	TGTGGTGCCAGATCTTCTCCATGT
AFP	Afp–F	GGAAGCATGTTAAATGAGCATG
	Afp–R	AGGGCCAGCTTCTGAAT
α-SMA	ACTA2–F	ATTGTGCTGGACTCTGGAGATGGT
	ACTA2–R	TGATGTCACGGACAATCTCACGCT